Role of excitons in double Raman resonances in GaAs quantum wells

L. Viña and J. M. Calleja
Instituto Nicolás Cabrera, Facultad de Ciencias C-IV, Universidad Autónoma de Madrid, Cantoblanco, E-28049 Madrid, Spain

A. Cros and A. Cantarero
Departamento de Física Aplicada, Universidad de Valencia, Dr. Moliner 50, Burjasot, E46100 Valencia, Spain

T. Berendschot and J. A. A. J. Perenboom
High Field Magnet Laboratory, University of Nijmegen, Toernooiveld NL-6525 ED, Nijmegen, The Netherlands

K. Ploog
Paul-Drude-Institut für Festkörperelektronik, Hausvogteiplatz 5-7, D-10117 Berlin, Federal Republic of Germany
(Received 2 August 1995)

Raman scattering by longitudinal-optical phonons has been measured in GaAs-AlAs multiple quantum wells at high magnetic fields. Doubly resonant scattering processes are observed at photon energies corresponding to magneto-excitons with different principal quantum numbers for the incoming and outgoing channels. The existence of these initially forbidden scattering processes, their resonance energies, and their relative intensities are correctly reproduced by our theoretical description. The model takes into account the excitonic nature of the intermediate states, as well as scattering processes involving a nonzero in-plane phonon wave vector, which is required to allow inter-Landau level scattering of the exciton.

I. INTRODUCTION

Inelastic light scattering in two-dimensional (2D) semiconductor systems has been widely and successfully used in the last years to probe their vibrational properties and electronic excitations.[1,2] When the energy of the incident or the scattered light equals some real transition of the system, a resonant enhancement of the scattering cross section, known as incoming and outgoing resonances, respectively, occurs.[3] Their study gives valuable information on the electronic structure of semiconductor quantum wells (QW's) and superlattices. Resonant Raman scattering (RRS) by longitudinal-optical (LO) phonons in 2D systems is generally stronger than in bulk materials due to the enhanced excitonic effects in 2D. RRS profiles in 2D can be tailored in specific ways due to changes in the electronic structure of the system by quantum confinement or by external fields. This flexibility allows us to obtain energy level configurations in which two electronic transitions of zero wave vector are separated by the LO phonon energy. If a scattering process is allowed in these conditions, it will be simultaneously resonant for incoming and outgoing channels. These doubly resonant Raman scattering (DRRS) processes are observed as a strong enhancement of the scattering intensity. This enhancement is due to the simultaneous vanishing of the two energy denominators appearing in the third-order perturbation theory expression of the Raman cross section.[3] DRRS has been first observed in bulk GaAs (Ref. 4) using uniaxial stress to split the heavy hole (hh) and light hole (lh) valence states by the LO phonon energy. In 2D semiconductor systems DRRS conditions have been met by a careful control of the confinement[5,6] or applying external electric[7] or magnetic[8,9] fields.

In a magnetic field the electronic states form discrete Landau levels (LL's) whose energies are directly proportional to the field. It is then possible to meet DRRS conditions by matching the LL separation to the LO phonon energy. Magnetic-field-induced DRRS have been observed in bulk GaAs,[10] which are correctly interpreted in terms of hole scattering with all the electronic states involved belonging to the same LL.[11] In 2D the situation is more controversial: the experimental results on GaAs-AlAs multiple quantum wells reported up to 13 T (Ref. 8) show that the incoming and outgoing channels of the DRRS process belong to different LL's. This process is forbidden in the independent electron-hole pair picture, so that excitons were suggested as the intermediate states in the scattering process. Furthermore, calculations on the absolute magneto-Raman cross sections,[12] *excluding excitonic effects* but taking explicitly into account the 2D valence-band structure, did not reproduce either the experimental energy positions of the different DRRS structures or their polarization selection rules.

In this paper we present experimental and theoretical results to overcome the actual controversy. Measurements have been done at high magnetic fields,[9] which reveal DRRS peaks involving different LL's. They correspond to energies and magnetic fields expected from the extrapolation of the low-field results.[8] The RRS intensity has been also calculated as a function of magnetic field for different light polarizations, assuming exciton-phonon scattering processes. To account for inter-LL scattering of excitons a finite in-plane wave vector is required in our model to break the selection rules. In our experimental conditions it can be provided by interface roughness.

Under these assumptions, we find an excellent agreement between the theoretical and experimental results on the values of the magnetic field and photon energies at which

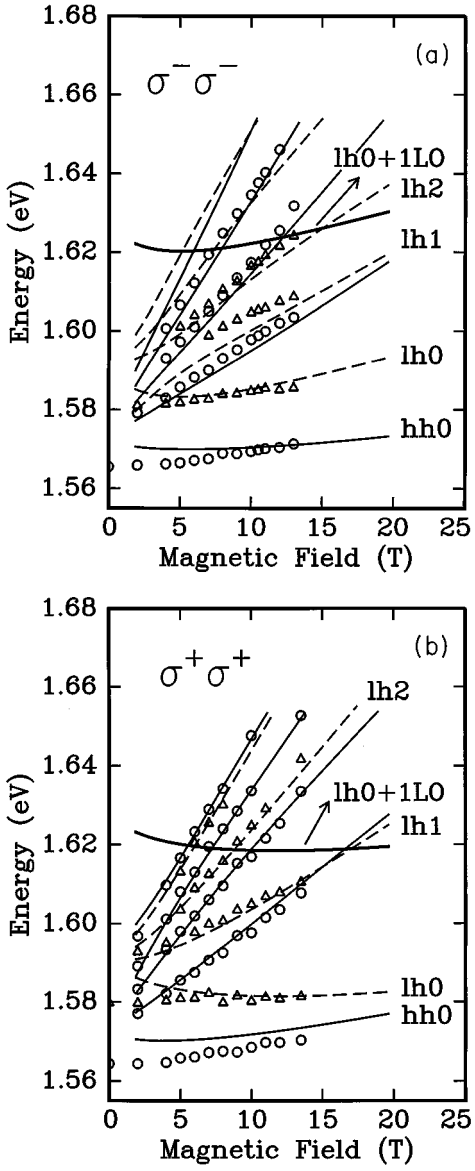

FIG. 1. Energy transitions as a function of magnetic field measured by PLE for (a) σ^- and (b) σ^+ polarization configurations. Circles correspond to transitions related to the hh and triangles are related to the lh.

DRRS occur, as well as on their polarization dependence and relative intensities.

The paper is organized as follows: Section II gives a brief description of the experimental setup. In Sec. III the theoretical model for the Raman scattering efficiency is developed. After calculating the energy levels of electron-hole pairs in a magnetic field a magneto-excitonic model, including Coulomb interaction up to second order in perturbation theory, is used to calculate the Raman scattering efficiency. The experimental results and the discussion under the light of the previously developed model is given in Sec. IV, while Sec. V summarizes the main results of the work.

II. EXPERIMENTAL DETAILS

The samples studied are GaAs-AlAs multiple quantum wells grown in the (001) direction by molecular-beam epitaxy. The width of wells and barriers is 100 Å. More details on sample preparation and characterization are given in Refs. 8 and 9. RRS experiments have been done in a bitter-coil 20-T magnet. The spectra were excited with a Ti-sapphire tunable laser and recorded with a triple spectrometer with multichannel detection. Polarization selection rules were studied using light circularly polarized by an achromatic $\lambda/4$ plate. The light was focused on and collected from the sample by a single lens of 3-mm focal length. At the highest fields, the Faraday rotation occurring at the lens produces some polarization mixing that prevents the observation of clear selection rules. All the measurements were performed at temperatures ranging from 2 to 4 K.

III. THEORETICAL MODEL

A magnetic field parallel to the QW growth direction (z axis) quantizes the electronic motion completely, changing the density of states and breaking the degeneracy of the QW subbands into Landau levels. This zero-dimensional density of states strongly increases the efficiency of the Raman process.[13] The Raman scattering efficiency per unit crystal length and solid angle for the emission of one phonon is related to the probability amplitude of the process, W_{FI}, by the expression

$$\frac{dS}{d\Omega}=\frac{\omega_L\omega_S^3\eta_S\eta_L}{(2\pi)^2c^4}\frac{V}{(\hbar\omega_L)^2}|W_{FI}(\omega_S,\vec{e}_S;\omega_L,\vec{e}_L)|^2 \times[n(\omega_q)+1], \tag{1}$$

where $\omega_{L(S)}$, $\eta_{L(S)}$, and $\vec{e}_{L(S)}$ are the angular frequency, refractive index, and polarization wave vector of the incident (scattered) photon. The last term, which includes the Bose-Einstein phonon occupation factor, $n(\omega_q)$, represents the number of phonons with frequency ω_q present in the crystal at a given temperature.

For a one-phonon emission process, keeping only the most resonant term, we can use third-order perturbation theory to write the scattering amplitude as

$$W_{FI}=\sum_{\alpha,\beta}\frac{\langle 0|\hat{H}_{\rm ER}|\beta\rangle\langle\beta|\hat{H}_{\rm EP}|\alpha\rangle\langle\alpha|\hat{H}_{\rm ER}|0\rangle}{(\hbar\omega_S-E_\beta+i\Gamma_\beta)(\hbar\omega_L-E_\alpha+i\Gamma_\alpha)}, \tag{2}$$

where $|\alpha\rangle$ ($|\beta\rangle$) is the intermediate excitonic states with energy $E_{\alpha(\beta)}$ and lifetime broadening $\Gamma_{\alpha(\beta)}$. The Hamiltonians $H_{\rm ER}$ and $H_{\rm EP}$ describe the exciton-radiation and exciton-phonon interactions, respectively.

To evaluate Eq. (2), the following steps will be performed: (i) we determine the energy levels adjusting the effective masses and g factors to the experimental values by a 4×4 Luttinger Hamiltonian. (ii) Using the previously determined parameters, we construct realistic wave functions in a parabolic approximation including Coulomb interaction. (iii) Finally, we use these wave functions to compute electron-phonon and electron-radiation matrix elements and determine the Raman scattering efficiency.

A. Energy levels in a magnetic field

Figures 1(a) and 1(b) show the positions of the transition energies as a function of the magnetic field measured by photoluminescence excitation (PLE). Circles indicate transitions and are identified as having heavy hole (hh) character and triangles as those of light hole (lh) character. We have used a previously developed model (Ref. 14) to obtain information about the parameters describing the electronic bands in the sample (effective masses, energy levels and g factors). The proximity of the energy subbands in the valence-band edge of diamond and zinc-blende-type semiconductors changes the simple picture of regularly spaced Landau levels, leading to states of mixed heavy- and light-hole character. This has been taken into account by using a 4×4 Luttinger Hamiltonian for the hh and 1h subbands. The conduction band has been taken to be parabolic but anisotropic, with an electron mass that depends on the QW subband energy, as explained in Ref. 15. In order to obtain the band parameters correctly, we have taken into account, in a simple way, the influence of the electron-hole Coulomb interaction on the interband magneto-optical transitions. We have used a two-dimensional excitonic model for the binding energy E_B, describing the partial confinement of the exciton in the QW by introducing a dimensionality parameter D (Ref. 16):

$$E_B \approx 3D\left[\frac{\hbar eB}{4\mu_{xy}^h R(n+1/2)}\right]^{1/2} R, \tag{3}$$

where $R=\mu_{xy}^h e^4/2\hbar^2\varepsilon^2$ is the effective Rydberg, ε the dielectric constant of the GaAs layer, and $\mu_{xy}^h = m_{xy}^h m_{xy}^e/(m_{xy}^h+m_{xy}^e)$ the exciton in-plane reduced mass, with h=hh, lh for heavy-hole or light-hole excitons, respectively. n represents the Landau quantum number. The value of the parameter D changes from 1/4 for a three-dimensional exciton to 1 for a two-dimensional system, and has been taken to be the same for heavy-hole and light-hole states for the sake of simplicity. In this way, the ground and excited states of hh and lh excitons are simultaneously fitted with only two free parameters: the in-plane electron effective mass m_{xy}^e and the dimensionality parameter D. The energies of the electron-hole transitions obtained within this approximation[12] are represented in Figs. 1(a) and 1(b) with full and dashed lines for the hh and lh levels, respectively. The valence-band g factors are now easily obtained from the energy difference between corresponding levels of the two spin orientations represented in Figs. 1(a) and 1(b). The in-plane electron effective mass (m_{xy}^e), the dimensionality parameter D, and the g factors obtained from the fitting are summarized in Table I. These parameters coincide with those reported in Ref. 14 for a similar sample.

Besides changing the effective masses and g factors of the different heavy- and light-hole states, the effect of valence-band mixing is to give rise to new transitions involving LL's with different indices. The oscillator strengths of these transitions are much smaller than the ones corresponding to the levels shown in Figs. 1(a) and 1(b) and they have been omitted for clarity.[19,20] As the transitions have not been observed in the experiments, we will also neglect them in the calculation of the Raman scattering efficiency. In order to go further with our model of magnetoexcitons, we will describe the valence band within a parabolic model.

TABLE I. Parameters used in the calculation of the Landau levels and Raman scattering efficiency in GaAs/AlAs QW's.

Parameters	Values	Reference
$\hbar\omega_g$(GaAs)	1.520 eV	17
$\hbar\omega_g$(AlAs)	3.13 eV	17
Γ	1 meV	
d	92 Å	
m_z^e	$0.067m_0$	$\vec{k}\cdot\vec{p}$ calculation (Ref. 15)
m_z^{hh}	$0.34m_0$	14
m_z^{lh}	$0.094m_0$	$\vec{k}\cdot\vec{p}$ calculation (Ref. 15)
m_{xy}^e	$0.076m_0$	From Fig. 1
μ_{xy}^{hh}	$0.059m_0$	$\vec{k}\cdot\vec{p}$ calculation (Ref. 14)
μ_{xy}^{lh}	$0.089m_0$	$\vec{k}\cdot\vec{p}$ calculation (Ref. 14)
γ_1	7.1	18
γ_2	2.1	18
γ_3	2.9	18
κ	1.2	17
$\hbar\omega_{LO}$	37 meV	14
Band offset(%)	0.70	14
D	0.7	From Fig. 1
g_{lh}^0	6.2	$\vec{k}\cdot\vec{p}$ calculation (Ref. 14)
g_{lh}^2	-12.6	$\vec{k}\cdot\vec{p}$ calculation (Ref. 14)

B. Eigenstates: Effect of Coulomb interaction

To take profit of the cylindrical symmetry of the QW system, we express the position of the electron (hole) in cylindrical coordinates, $(\vec{r}_{e(h)}, z_{e(h)})$, and write the vector potential associated to the magnetic field in the symmetric gauge:

$$\vec{A}=\frac{1}{2}\vec{B}\times\vec{r}. \tag{4}$$

Using the gauge transformation introduced by Yang and Sham,[19] we can write the exciton Hamiltonian and wave functions in terms of the relative and center-of-mass motion of the electron-hole pair in the x-y plane: $\vec{r}=\vec{r}_h-\vec{r}_e$ and $\vec{R}=(m_{xy}^e\vec{r}_e+m_{xy}^h\vec{r}_h)/(m_{xy}^e+m_{xy}^h)$. In the dipole approximation the wave vector of the center-of-mass motion of the exciton vanishes, and the Hamiltonian of the magnetoexciton in the QW is given by

$$\begin{aligned} H_{\rm exc}^h = &-\frac{\hbar^2}{2}\frac{\partial}{\partial z_e}\frac{1}{m_z^e}\frac{\partial}{\partial z_e}+V(z_e)-\frac{\hbar^2}{2}\frac{\partial}{\partial z_h}\frac{1}{m_z^h}\frac{\partial}{\partial z_h}+V(z_h)\\ &-\frac{\hbar^2}{2\mu_{xy}^h}\frac{1}{r}\frac{\partial}{\partial r}\left(r\frac{\partial}{\partial r}\right)-\frac{\hbar^2}{2\mu_{xy}^h}\frac{1}{r^2}\frac{\partial^2}{\partial\phi^2}\\ &+\frac{1}{2i}\hbar\frac{\mu_{xy}^h}{\mu_-^h}\omega_c^h\frac{\partial}{\partial\phi}+\frac{\mu_{xy}^h(\omega_c^h)^2}{8}r^2+V_C(r,z_e-z_h), \end{aligned} \tag{5}$$

where $\omega_c^h = eB/\mu_{xy}^h$ is the cyclotron frequency of the exciton and $\mu_-^h = m_{xy}^h m_{xy}^e/(m_{xy}^h - m_{xy}^e)$. This Hamiltonian can be written as a sum of three contributions:

$$H_{\rm exc} = H_{\rm QW} + H_B + V_C(r, z_e - z_h). \tag{6}$$

$H_{\rm QW}$ corresponds to the first four terms and represents the motion along the z axis, including the QW confining potential in the conduction and valence bands. H_B describes the motion in the xy plane and the interaction with the magnetic field. The last term, $V_C(r, z_e - z_h)$, is the electron-hole Coulomb interaction. The exact eigenvalues of the Hamiltonian including magnetic field, band mixing effects, and Coulomb interaction are very difficult to obtain, and different approximations have been considered, depending on the characteristics of the system under study and the relative importance of the magnetic field and Coulomb effects.[16,21–23]

We will take into account the confinement of the excitonic movement along the quantum well direction and neglect the z dependence of the Coulomb potential, writing

$$V_C = -\frac{e^2}{\varepsilon r}. \tag{7}$$

With this approximation the exciton is considered to be completely confined in the QW. This interaction will be treated as a perturbation to the motion of the electron-hole pair under the magnetic field. It is justified for high enough magnetic fields, that is, when the cyclotron radius is smaller than that of the exciton (around 8 T for GaAs), and becomes better for excited excitonic states. We can then separate the motion in the growth and in-plane directions and factorize the exciton function:

$$\psi(r, z_h, z_e) = \phi_{\nu_e}(z_e)\,\phi_{\nu_h'}(z_h)\,\Phi_{n,l}^0(r, \phi), \tag{8}$$

where $\phi_{\nu_{e(h)}}(z_{e(h)})$ represents the confinement of the electron (hole) by the QW conduction (valence) band profile corresponding to the νth quantized subband.[15] The function $\Phi_{n,l}^0$ is a simultaneous eigenfunction of the magnetic field Hamiltonian, H_B, and the angular momentum operator $L = -i\hbar\partial/\partial\phi$, with eigenvalue $\hbar l$, and describes the relative in-plane motion of the electron-hole pair in the magnetic field with quantum numbers l and n. In polar coordinates it can be written as[22]

$$\Phi_{n,l}^0 = \sqrt{\frac{(n+|l|)!}{n!\,\pi(2\lambda^2)^{|l|+1}}}\,\frac{1}{|l|!}\,e^{il\phi} r^{|l|} e^{-r^2/4\lambda^2} \times M\left(-n, |l|+1, \frac{r^2}{2\lambda^2}\right), \tag{9}$$

where $\lambda = \sqrt{\hbar/eB}$ is the magnetic length and $M(-n, |l|+1, x)$ represents the confluent hypergeometric function.

The energy of the free electron-hole pair is given as a function of four quantum numbers, ν_e, ν_h, n, and l:

$$E_{\nu_e,\nu_h,n,l}^0 = E_{\nu_e} + E_{\nu_h} + E_g + \hbar\omega_c^h\left(n + \frac{|l|+1}{2} - \frac{\mu_{xy}^h}{\mu_-^h} l\right). \tag{10}$$

To calculate the exciton eigenfunctions and eigenvectors we use perturbation theory up to second order for the Coulomb terms:

$$E_{\nu_e,\nu_h,n,l} = E_{\nu_e,\nu_h,n,l}^0 + \langle \Phi_{n,l}^0 | V_C | \Phi_{n,l}^0 \rangle + \sum_{n' \neq n} \frac{|\langle \Phi_{n',l}^0 | V_C | \Phi_{n,l}^0 \rangle|^2}{E_{n,l}^0 - E_{n',l}^0}, \tag{11}$$

$$\Phi_{n,l}^{(2)} = \Phi_{n,l}^0 + \sum_{n' \neq n} \frac{\langle \Phi_{n',l}^0 | V_C | \Phi_{n,l}^0 \rangle}{E_{n,l}^0 - E_{n',l}^0} \Phi_{n',l}^0 + \sum_{\substack{n' \neq n \\ n'' \neq n}} \frac{\langle \Phi_{n',l}^0 | V_C | \Phi_{n'',l}^0 \rangle \langle \Phi_{n'',l}^0 | V_C | \Phi_{n,l}^0 \rangle}{(E_{n,l}^0 - E_{n',l}^0)(E_{n,l}^0 - E_{n'',l}^0)} \Phi_{n',l}^0, \tag{12}$$

where we have omitted the indices ν_e and ν_h in the expression of the unperturbed energies, because the two-dimensional Coulomb interaction does not connect the different QW subbands. As a consequence of the Coulomb interaction the different Landau levels get mixed, and their energies decrease by an amount that is proportional to the square root of the magnetic field. The only wave functions needed to evaluate the scattering efficiency are those with $l = 0$ [see Eqs. (15) and (16) below]. In this case, the matrix elements of the Coulomb interaction in Eq. (12) are given by the following analytical expression:

$$\begin{aligned} \langle \Phi_{n,0}^0 | V_C | \Phi_{m,0}^0 \rangle &= \langle \Phi_{m,0}^0 | V_C | \Phi_{n,0}^0 \rangle \\ &= \frac{e^2}{\sqrt{2}\lambda\varepsilon} \sum_{i=0}^{n} (-1)^i \binom{n}{i} \frac{1}{i!} \frac{\Gamma(i+1/2)\Gamma(1/2+m-i)}{\Gamma(m+1)\Gamma(1/2-i)}, \end{aligned} \tag{13}$$

with $n \leqslant m$. The set of wave functions obtained by Eq. (12) is not orthogonal. Thus, we have orthogonalized them using the Gramm-Smith method,[24] which gives us the final wave functions $\Phi_{n,l}$ as a combination of $\Phi_{n,l}^{(2)}$. However, since the $\Phi_{n,l}^{(2)}$ functions are linear combinations of the unperturbed $\Phi_{n,l}^{(0)}$'s, the final result can be more conveniently written as

$$\Phi_{n,l} = \sum_m C_{n,m} \Phi_{m,l}^0. \tag{14}$$

To obtain the Raman scattering efficiency, we need to calculate the matrix elements of the interaction Hamiltonians that appear in the definition of the scattering amplitude Eq. (2).

C. Matrix elements

The exciton-radiation matrix element is given by

$$-\frac{e}{m}\left(\frac{2\pi\hbar}{\omega\eta^2}\right)^2 (\vec{e}\cdot\vec{p}_{cv_h}) f_{\nu_e,\nu_h} \Phi_{n,l}(0), \tag{15}$$

where the exciton function evaluated at $\vec{r} = 0$ is given by

$$\Phi_{n,l}(r=0)=\frac{1}{\sqrt{2\pi}\lambda}\delta_{l,0}\sum_m C_{n,m} \tag{16}$$

and $f_{\nu_e,\nu_h}=\langle\phi_{\nu_e}(z_e)|\phi_{\nu_h}(z_h)\rangle$ is the overlap integral between the envelope functions of the conduction and valence QW subbands ν_e and ν_h, respectively. Therefore, only excitons with zero angular momentum and with conduction and valence QW subbands corresponding to the same parity will contribute to the Raman spectra.

The electron-phonon matrix element is given by

$$\langle\beta|\hat{H}_{\rm EP}|\alpha\rangle=\langle\beta|\sum_{\vec{q}_{xy}}\sum_{p=1}^{N}\frac{C_F}{q}\sqrt{\omega_{\rm LO}}\omega_q\{e^{-i\vec{q}_{xy}\vec{r}_e}\chi_{p,\vec{q}_{xy}}(z_e)-e^{-i\vec{q}_{xy}\vec{r}_h}\chi_{p,\vec{q}_{xy}}(z_h)\}|\alpha\rangle, \tag{17}$$

where $\omega_q^2=\omega_{\rm LO}^2-\beta_s^2q^2$ represents the phonon dispersion in the QW, β_s is a constant with units of velocity, and $\omega_{\rm LO}$ the LO phonon bulk frequency. The phonon wave vector has been separated in two components:

$$q^2=q_{xy}^2+q_z^2, \tag{18}$$

where the component along the growth direction is quantized and is given by $q_z=p\pi/d$, where p is an integer and d is the width of the quantum well. The constant C_F is defined as

$$C_F=-i\hbar\omega_{\rm LO}\left(\frac{4\pi\alpha\not\ell}{V_0}\right)^{1/2}, \tag{19}$$

$$\alpha=\frac{e^2}{2\hbar\omega_{\rm LO}\not\ell}\left(\frac{1}{\varepsilon_\infty}-\frac{1}{\varepsilon_0}\right),\quad \not\ell=\left(\frac{\hbar}{2m_0\omega_{\rm LO}}\right)^{1/2}, \tag{20}$$

where ε_∞ and ε_0 are the optical and static dielectric constants, respectively.

In a 1LO Raman process mediated by the Fröhlich interaction, only even phonon modes are excited and the z dependence of the Fröhlich Hamiltonian is given by

$$\chi_{p,\vec{q}_{xy}}(z)=\begin{cases}e^{q_{xy}z}\sin(q_{xy}d/2), & z\leqslant -d/2\\ (-1)^{p/2}\cos(p\pi/d)z-e^{-q_{xy}d/2}\cos(q_{xy}d/2), & -d/2<z<d/2\\ e^{-q_{xy}z}\sin(q_{xy}d/2), & d/2\leqslant z.\end{cases} \tag{21}$$

The function $\chi_{p,\vec{q}_{xy}}(z)$ is taken from the expression given by Trallero-Giner and Comas.[25,26]

Using the obtained wave functions and energies, the probability amplitude of the scattering process [Eq. (2)] can be written as

$$W_{FI}=\sum_{\substack{n,n',h\\ \nu,\nu'}}(\vec{e}_S^{\,*}\cdot\vec{p}_{cv_h})(\vec{e}_L\cdot\vec{p}_{cv_h})\frac{4e^2\hbar}{\pi m_0^2}\frac{C_F}{\sqrt{\omega_S\omega_L}\eta_S\eta_L d}\frac{1}{q}\sqrt{\frac{\omega_{\rm LO}}{\omega_q}}$$
$$\times f_{\nu_e,\nu_h}f_{\nu_e',\nu_h'}\lambda\Phi_{n,0}^h\lambda\Phi_{n',0}^h\frac{g_{\nu_e,\nu_e'}(q)I_{n,n'}^h(-q_h)-g_{\nu_h,\nu_h'}(q)I_{n,n'}^h(-q_e)}{(\hbar\omega_S-E_{\nu_e,\nu_h,n,0}+i\Gamma)(\hbar\omega_L-E_{\nu_e',\nu_h',n',0}+i\Gamma)}, \tag{22}$$

where $q_{e(h)}=q_{xy}m_{xy}^{e(h)}/(m_{xy}^e+m_{xy}^h)$, the function $g_{\nu,\nu'}(q)$ is the electron-phonon interaction matrix element in the growth direction, defined as

$$g_{\nu,\nu'}(q)=\frac{\pi}{2}\int_{-\infty}^{\infty}\phi_\nu(z)\chi_{p,\vec{q}_{xy}}(z)\phi_{\nu'}(z)dz, \tag{23}$$

and $I_{n,n'}^h(q_\zeta)$ represents the in-plane exciton-phonon interaction:

$$I_{n,n'}^h(q_\zeta)=\int\Phi_{n,0}^h e^{-i\vec{q}_\zeta\cdot\vec{r}}\Phi_{n',0}^h d^3r. \tag{24}$$

For simplicity, we have used a constant lifetime broadening parameter Γ. The dependence of the matrix elements $I_{n,n'}^h(q_\zeta)$ on the dimensionless product λq_{xy} is shown in Figs. 2(a) and 2(b) for the transitions $n=0\rightarrow n=1$ and $n=0\rightarrow n=2$, respectively. Excitons of two types have been considered, $h=$lh (full and dashed-dotted lines) and $h=$hh (dashed and dotted lines). In each case the phonon can be scattered either by the hole ($\zeta=h$, shown in full and dashed lines) or by the electron ($\zeta=e$ in dashed-dotted and dotted lines). The functions start from zero and present oscillations as λq_{xy} increases. Due to the smaller in-plane mass of the electron, the matrix elements for $\zeta=e$ present a smooth variation with λq_{xy}. On the other hand, when the phonon is

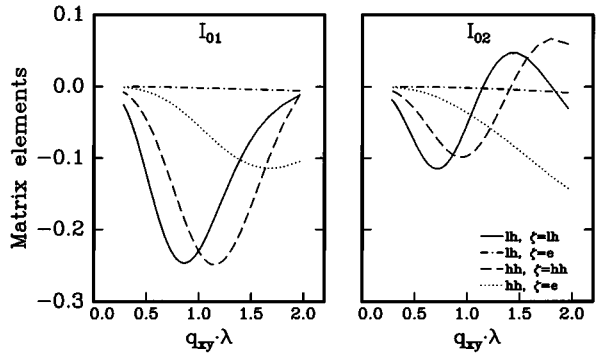

FIG. 2. In-plane part of the exciton-phonon interaction as a function of $q_{xy}\lambda$. (a) corresponds to the $n=0$ to $n=1$ and (b) to the $n=0$ to $n=2$ transitions. The different curves refer to lh or hh excitons and scattering events occurring in the valence ($\zeta=$hh, lh) or conduction ($\zeta=e$) bands.

emitted by the hole, the oscillations have a maximum around $\lambda q_{xy}=1$. This is the value for which the matrix elements give the most important contribution to the probability amplitude.

Finally, the Raman scattering efficiency, Eq. (1), can be written as

$$\frac{dS}{d\Omega}=\frac{\omega_S}{\omega_L}\left(\frac{\ell}{d}\right)^2\frac{\omega_{\mathrm{LO}}}{\omega_q}\frac{1}{\ell^2 q^2}\left(\sum_{\substack{n,n',h\\ \nu,\nu'}} S_0^h\Theta\right)^2, \tag{25}$$

where, to simplify the expression, we have defined the function Θ:

$$\Theta=f_{\nu_e,\nu_h}f_{\nu_e',\nu_h'}\lambda\Phi^h_{n,0}\lambda\Phi^h_{n',0}\omega^2_{\mathrm{LO}} \times\frac{g_{\nu_e,\nu_e'}(q)I^h_{n,n'}(-q_h)-g_{\nu_h,\nu_h'}(q)I^h_{n,n'}(-q_e)}{(\hbar\omega_S-E_{\nu_e,\nu_h,n,0}+i\Gamma)(\hbar\omega_L-E_{\nu_e',\nu_h',n',0}+i\Gamma)}, \tag{26}$$

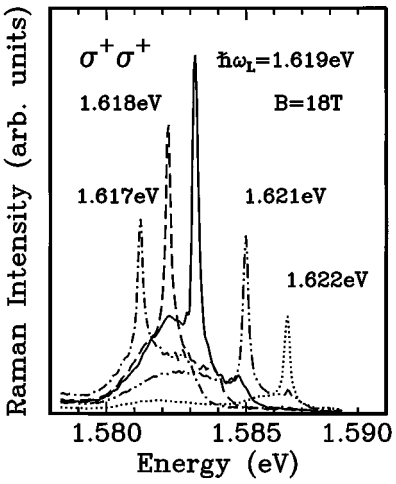

FIG. 3. Raman spectra taken at 18 T in $\sigma^+\sigma^+$ polarization configuration for different incident laser energies. The energies and the magnetic field are chosen to be in the proximity of a double resonance with lh1 and lh0 as incoming and outgoing channels, respectively.

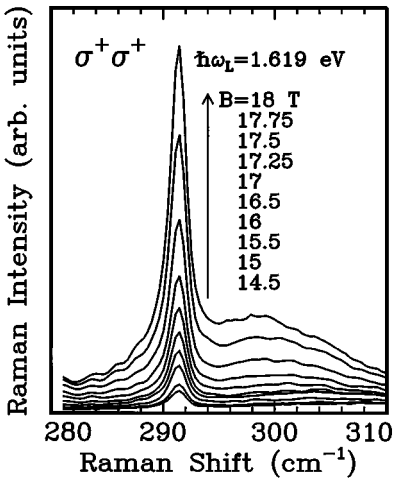

FIG. 4. Raman spectra, taken with a laser energy of 1.619 eV, for different magnetic fields. The sequence corresponds to a double resonance with lh1 and lh0 as incoming and outgoing channels, respectively.

and the constant S_0^h:

$$S_0^h=\left(\frac{\omega_S}{\omega_L}\frac{\eta_S}{\eta_L}\alpha\ell\right)^{1/2}\frac{e^2}{m^2c^2\hbar^2\omega_{\mathrm{LO}}}(\vec{e}_S^{\,*}\cdot\vec{p}_{cv_h})(\vec{e}_L\cdot\vec{p}_{cv_h}). \tag{27}$$

IV. RESULTS AND DISCUSSION

Figure 3 shows the measured Raman spectra for a magnetic field of 18 T in the $\sigma^+\sigma^+$ polarization configuration. The different traces correspond to energies around the outgoing resonance condition involving the ground lh state [energies labeled lh0+1LO, plotted with a thick line in Fig. 1(b)]. The GaAs LO phonon is seen on top of a broad background corresponding to the photoluminescence of the lh0 state. The resonant behavior of the phonon peak is clearly illustrated as the incoming laser energy changes around 1.619 eV, its intensity decreasing for energies lower and higher than this value. The double resonant character of this intensity enhancement is demonstrated in Fig. 4, where we have represented the same kind of spectra as in Fig. 3, but keeping this time the laser energy constant and changing the magnetic field from 14.5 to 18 T. As can be seen in Fig. 1(b), the energy of the lh0 state remains practically constant for this field range, and the outgoing resonance is satisfied for every value of the magnetic field. However, Fig. 4 reveals a strong dependence of the intensity of the resonance when the magnetic field is changed, that is, when the laser energy (thick line in Fig. 1) crosses the lh1 energy transition. This response confirms that the Raman peak corresponds to a double resonance, with the lh1 state as incoming channel and lh0 as outgoing. The same behavior is reproduced when the magnetic field and laser energy are simultaneously tuned with the lh2 state as incoming channel and lh0 as outgoing. Similar double resonant enhancements are also observed, for the appropriate values of energy and magnetic field, for the other polarization configuration.

In order to study the double resonant behavior as a function of the magnetic field we have proceeded in the follow-

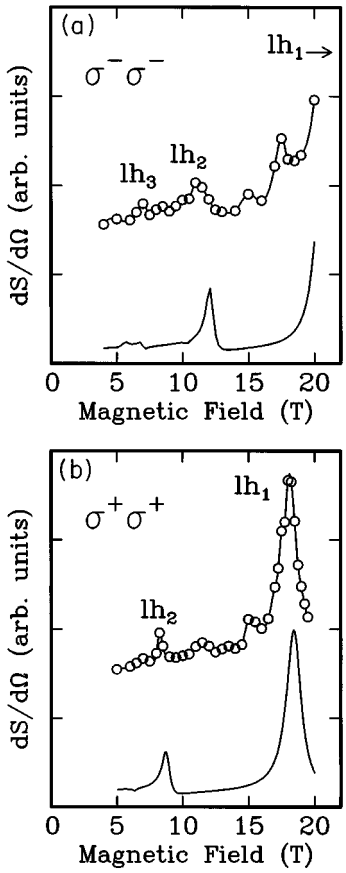

FIG. 5. Raman scattering efficiency as a function of magnetic field for (a) $\sigma^-\sigma^-$ and (b) $\sigma^+\sigma^+$ parallel polarization configurations in backscattering geometry. The experimental points (circles) have been plotted on top of the theoretical lines for comparison. The labels indicate the incoming channels of the double resonances.

ing way. At different fixed magnetic fields, we have measured the Raman spectra in the proximity of the double resonances, as shown in Fig. 3 for 18 T. In this way we obtain an accurate value of the maximum intensity of the LO phonon peak for each magnetic field. This procedure allows us to eliminate the influence of the luminescence background, which can be easily subtracted. The results are plotted as empty circles in Figs. 5(a) and 5(b) for $\sigma^-\sigma^-$ and $\sigma^+\sigma^+$ polarization configurations, respectively. The peaks correspond to double resonances for the incoming lh*n* and outgoing lh0 channels. The peak appearing around 18 T in Fig. 5(a) is due to polarization leakage from $\sigma^+\sigma^+$ configuration. Their observation indicates that the electron-phonon interaction is responsible for an arbitrary change in the magnetoexciton principal quantum numbers. This implies that the Fröhlich interaction allows for scattering between states of the same subband with $\Delta n \neq 0$.

Previous attempts to explain these double resonances by means of a free electron-hole pair model did not reproduce the experimental values of both position and intensity of the double resonances. Therefore, we have used in this work an excitonic model to obtain the correct energy transitions. However, in strict backscattering configuration the wave-vector conservation allows only phonons with $q_{xy}=0$ to be excited. In this situation the exciton-phonon interaction is not able to connect different excitonic states, since they are mutually orthogonal. Thus we must allow for scattering by phonons with a nonzero in-plane phonon wave vector, which can be attributed to interface roughness.[27] In our calculations we have taken an effective value of q_{xy} of the order of the inverse of the exciton radius.

The Raman scattering efficiency calculated with this model is represented in Figs. 5(a) and 5(b) (solid lines) for both parallel circular polarization configurations. The result is shown under the experimental points for comparison. The excellent agreement between theory and experiments demonstrates the adequacy of our theoretical model and the necessity of including excitonic effects, as well as q nonconservation, for a correct description of the observed double resonances.

V. CONCLUSIONS

We have studied double resonances in the first-order Raman scattering induced by a magnetic field in semiconductor quantum wells. We have shown the necessity to consider excitonic effects to understand the correct energy positions, magnetic field values, intensities, and polarization selection rules of these resonances. A calculation of the Raman efficiency taking into account interface roughness scattering and electron-hole Coulomb interaction explains all the experimental features.

ACKNOWLEDGMENTS

We are indebted to C. Tejedor for seminal ideas for this work. The work has been partially supported by the Projects No. PB93-0687 of DGICYT, No. MAT94-0982-C02-01 of CICYT, and No. CHRX-CT92-62 (MagNET) of the European Communities.

[1] *Light Scattering in Solids V*, edited by M. Cardona and G. Güntherodt, Topics in Applied Physics Vol. 66 (Springer, Berlin, 1989).

[2] A. Pinczuk, S. Schmitt-Rink, G. Danan, J. P. Valladares, L. N. Pfeiffer, and K. W. West, Phys. Rev. Lett. **63**, 1633 (1989); A. Pinczuk, B. S. Dennis, L. N. Pfeiffer, and K. W. West, *ibid.* **70**, 3983 (1993).

[3] *Light Scattering in Solids II*, edited by M. Cardona and G. Güntherodt, Topics in Applied Physics Vol. 51 (Springer, Berlin, 1982.)

[4] F. Cerdeira, E. Anastassakis, W. Kauschke, and M. Cardona, Phys. Rev. Lett. **57**, 3209 (1986).

[5] R. C. Miller, D. A. Kleinman, C. W. Tu, and S. K. Sputz, Phys. Rev. B **34**, 7444 (1986).

[6] D. A. Kleinman, R. C. Miller, and A. C. Gossard, Phys. Rev. B **35**, 664 (1987).

[7] F. Agulló-Rueda, E. E. Mendez, and J. M. Hong, Phys. Rev. B **38**, 12 720 (1988).
[8] F. Calle, J. M. Calleja, F. Meseguer, C. Tejedor, L. Viña, C. López, and K. Ploog, Phys. Rev. B **44**, 1113 (1991); F. Calle, J. M. Calleja, C. Tejedor, L. Viña, and K. Ploog, Surf. Sci. **267**, 418 (1992).
[9] J. M. Calleja, L. Viña, T. Berendschot, F. Calle, C. López, F. Meseguer, C. Tejedor, and J. A. A. J. Perenboom, in *Phonons in Semiconductor Nanostructures*, Vol. 236 of *NATO Advanced Study Institute, Series E*, edited by J. P. Leburton, J. Pascual, and C. R. Sotomayor-Torres (Kluwer, Dordrecht, 1993), p. 121.
[10] T. Ruf, R. T. Phillips, C. Trallero-Giner, and M. Cardona, Phys. Rev. B **41**, 3039 (1990).
[11] C. Trallero-Giner, T. Ruf, and M. Cardona, Phys. Rev. B **41**, 3028 (1990).
[12] A. Cros, A. Cantarero, C. Trallero-Giner, and M. Cardona, Phys. Rev. B **45**, 6106 (1992).
[13] V. I. Belitskii, A. V. Gol'tsev, I. G. Lang, and S. T. Pavlov, Fiz. Tverd. Tela (Leningrad) **25**, 1224 (1983) [Sov. Phys. Solid State **25**, 703 (1983)].
[14] A. Cros, T. Ruf, J. Spitzer, M. Cardona, and A. Cantarero, Phys. Rev. B **50**, 2325 (1994).
[15] G. C. La Rocca and M. Cardona, Phys. Status Solidi B **167**, 115 (1991).
[16] O. Akimoto and H. Hasegawa, J. Phys. Soc. Jpn. **22**, 181 (1967).
[17] *Physics of Group IV Elements and III-V Compounds*, edited by O. Madelung, M. Schulz, and H. Weiss, Landolt-Börnstein, New Series, Group III, Vol. 17, Pt. a (Springer-Verlag, Berlin, 1982), Chaps. 2.10 and 2.6.
[18] N. Binggeli and A. Baldereschi, Phys. Rev. B **43**, 14 734 (1991).
[19] S.-R. Eric Yang and L.J. Sham, Phys. Rev. Lett **58**, 2598 (1987).
[20] L. C. Andreani and A. Pasquarello, Phys. Rev. **42**, 8928 (1990).
[21] M. Altarelli and N. O. Lipari, Phys. Rev. B **7**, 3798 (1973).
[22] M. Altarelli and N. O. Lipari, Phys. Rev. B **9**, 1733 (1974).
[23] T. Yasui, Y. Segawa, Y. Aoyagi, Y. Iimura, G. E. W. Bauer, I. Mogi, and G. Kido, Phys. Rev. B **51**, 9813 (1995).
[24] *Quantum Mechanics*, edited by C. Cohen-Tannoudji, B. Diu, and Franck Laloë (Wiley, Paris, 1977).
[25] C. Trallero-Giner and F. Comas, Phys. Rev. B **37**, 4583 (1988).
[26] This phonon potential satisfies the electrostatic boundary conditions. Although the mechanical boundary conditions are strictly satisfied only if $q_{xy}=0$, the errors introduced for $q_{xy}\neq 0$ should remain small provided $q_{xy}<\pi/d$.
[27] A. J. Shields, C. Trallero-Giner, M. Cardona, H. T. Grahn, K. Ploog, V. A. Haisler, D. A. Tenne, N. T. Moshegov, and A. I. Toropov, Phys. Rev. B **46**, 6990 (1990).